



Article

Test Particles and Quasiperiodic Oscillations around Gravitational Aether Black Holes

Javlon Rayimbaev ^{1,2,3,4,*} , Farrux Abdulxamidov ^{5,6,7}, Sardor Tojiev ^{5,6}, Ahmadjon Abdujabbarov ^{3,4,6} , and Farhod Holmurodov ⁸

- ¹ Institute of Fundamental and Applied Research, National Research University TIIAME, Kori Niyoziy 39, Tashkent 100000, Uzbekistan
- ² School of Engineering, Central Asian University, Tashkent 111221, Uzbekistan
- ³ Faculty of Physics, National University of Uzbekistan, Tashkent 100174, Uzbekistan; ahmadjon@astrin.uz
- ⁴ Power Engineering Faculty, Tashkent State Technical University, Tashkent 100095, Uzbekistan
- ⁵ School of Mathematics and Natural Sciences, New Uzbekistan University, Mustaqillik Ave. 54, Tashkent 100007, Uzbekistan; sardor@astrin.uz (S.T.)
- ⁶ Ulugh Beg Astronomical Institute, Astronomy St. 33, Tashkent 100052, Uzbekistan
- ⁷ Institute of Nuclear Physics, Ulugbek 1, Tashkent 100214, Uzbekistan
- ⁸ Faculty of Mathematics, Namangan State University, Boburshoh Str. 161, Namangan 160107, Uzbekistan; hfarhod2024@gmail.com
- * Correspondence: javlon@astrin.uz

Abstract: This paper is devoted to the analysis of the dynamics of test particles in the vicinity of a black hole within the framework of a gravitational aether model. First, we explored the structure of spacetime by analyzing the curvature scalars. Then, we studied particle dynamics around a black hole using the Hamilton–Jacobi equation. The influence of the aether on the effective potential of the radial motion of test particles around the black hole has been investigated. The dependence of the innermost stable circular orbits (ISCO) on the aether parameter has also been investigated. We also considered particle collision near the black hole in the presence of aether, and studied the fundamental frequencies of the orbital motion of the test particles around the black hole in the presence of aether. Further, we applied the obtained results to the analysis of the upper and lower frequencies of twin-peaked quasiperiodic oscillations (QPOs) occurring near black holes. Finally, we use theoretical and numerical results to obtain constraints on model parameters using observation data in QPO.

Keywords: black holes; gravitational aether fields; test particles; particle collisions

PACS: 04.50.-h; 04.40.Dg; 97.60.Gb



Citation: Rayimbaev, J.; Abdulxamidov, F.; Tojiev, S.; Abdujabbarov, A.; Holmurodov, F. Test Particles and Quasiperiodic Oscillations around Gravitational Aether Black Holes. *Galaxies* **2023**, *11*, 95. <https://doi.org/10.3390/galaxies11050095>

Academic Editors: Fulai Guo and Yosuke Mizuno

Received: 8 May 2023

Revised: 10 August 2023

Accepted: 25 August 2023

Published: 1 September 2023



Copyright: © 2023 by the authors. Licensee MDPI, Basel, Switzerland. This article is an open access article distributed under the terms and conditions of the Creative Commons Attribution (CC BY) license (<https://creativecommons.org/licenses/by/4.0/>).

1. Introduction

The 21st century provided new discoveries in astrophysics, including the discovery of an accelerated expansion of the Universe. Within the standard theory of gravity, these phenomena can be modeled, including the cosmological constant to the corresponding solution of Einstein’s equation. Modern observations show that the dark energy responsible for the expansion and modeled by the cosmological constant constitutes 75% of the total mass of the Universe. However, models based on the cosmological constant have some fundamental problems. Particularly, in order to fit the observations, one should require an extreme fine-tuning of more than 60 orders of magnitude. Another open question is related to the value of the cosmological constant: why is its value minimal and not equal to zero?

In order to resolve the above-mentioned fundamental problems of the cosmological model based on the cosmological constant, several alternative models have been proposed. Authors of Ref. [1] proposed a gravity model applicable to cosmology. Cosmology based on the braneworld model was proposed in Ref. [2]. It is important to note that the majority

of alternative approaches aimed at resolving the cosmological constant problem involve modifications to Einstein's theory of gravity. These modifications often involve the inclusion of higher-order curvature terms in the geometric aspect of Einstein's equations.

In [3], a novel approach to modified gravity is proposed, introducing the concept of gravitational aether. The gravitational aether serves as a component to disentangle the vacuum of quantum field theory from gravity. According to this model, the right-hand side of the Einstein field equation (Equation (1)) is modified as follows:

$$(8\pi G')^{-1}G_{\mu\nu} = T_{\mu\nu} - \frac{1}{4}T_{\alpha}^{\alpha}g_{\mu\nu} + p(u_{\mu}u_{\nu} + g_{\mu\nu}), \quad (1)$$

and

$$\frac{d\phi}{dr} = \frac{M + 4\pi r^3 p}{r(r - 2M)}, \quad (2)$$

$$\frac{dp}{dr} = \frac{-p(M + 4\pi r^3 p)}{r(r - 2M)}, \quad (3)$$

Additionally, the Tolman–Oppenheimer–Volkoff equations are employed, represented by Equations (2) and (3), where p and ϕ denote the pressure and scalar potential of the field, respectively. These equations provide essential insights into the dynamics of the system under consideration.

The authors of [4] focused on the study of static black hole solutions within the gravitational aether framework. They argued that the aether couples the spacetime metric near the black hole horizon with the metric at infinity. By establishing this connection, they demonstrated the possibility of an accelerating cosmological solution far away from the black hole horizon. This intriguing relationship between the formation of stellar black holes and the expansion acceleration of the Universe holds the potential to address the coincidence problem by considering Planck-suppressed corrections within black hole physics.

When examining and testing gravity models and theories, it is crucial to establish an observational or experimental foundation. Analyzing the dynamics of test particles in the vicinity of a compact gravitating object described by the corresponding theory offers a valuable approach for developing new tests of gravity models [5,6].

Moreover, the utilization of X-ray observation data from astrophysical objects provides an avenue for constraining the physical parameters of the theory [7–10]. Additionally, the presence of the gravitational field affects the structure of the electromagnetic field, consequently influencing the behavior of charged particles [11–19]. Furthermore, the motion of magnetically charged particles and particles possessing nonzero magnetic dipole moments can provide valuable insight into the nature of the gravitational field surrounding compact objects [20–25].

Another interesting astrophysical phenomenon that can be used as a test of gravity models is quasiperiodic oscillations (QPOs). QPOs correspond to (several) peaks observed in radio- to X-ray bands of the electromagnetic spectrum. Special cases of QPOs, called twin peaked QPOs in microquasars, can be observed through the matter accreting into compact objects [26–30].

Numerous models have been proposed to explain the underlying mechanisms responsible for the generation of QPOs. Among these models, those based on the dynamics of test particles have shown significant promise. In particular, the harmonic oscillations exhibited by particles along radial, vertical, and azimuthal directions contribute to the observable QPO signals. By analyzing such models, investigations concerning the inner edge of the accretion disk around a compact object can be conducted [31,32]. The influence of gravity theories on QPO generation has been extensively explored in the literature [33–38].

This manuscript is structured as follows: Section 2 provides a brief description of the gravitational aether black hole solution, and Section 3 delves into the study of scalar invariants within the black hole spacetime. The dynamics of test particles around the black hole aether are investigated in Section 4, focusing on the influence of the aether field pres-

sure on particle energy, angular momentum, circular orbits, the innermost stable circular orbits (ISCOs), and energy efficiency of the Novikov–Thorne accretion disk. Additionally, we demonstrate how the aether field parameter mimics the spin of rotating Kerr black holes, yielding equivalent energy efficiencies. Section 9 explores test particle collisions and calculates the center-of-mass energy. The analysis of fundamental frequencies and their application to QPOs is presented in Section 7. Finally, we provide a summary of the results obtained.

In this study, we utilize a unit system where the speed of light c , and the gravitational constant G are set to unity, and we use a spacetime signature of $(-, +, +, +)$. The coordinates are chosen to be spherical (t, r, θ, φ) , and Greek indices range from 0 to 3. We follow the customary practice of summing over repeated indices in calculations.

2. Black Holes in the Gravitational Aether Theory

The static and spherical symmetric spacetime metric of the black hole with the total mass M in the gravitational aether model with the energy–momentum tensor given in (1) has the following form [4]

$$ds^2 = -e^{2\phi(r)} dt^2 + \left(1 - \frac{2M}{r}\right)^{-1} dr^2 + r^2 d\Omega^2 \quad (4)$$

where $d\Omega^2 = d\theta^2 + \sin^2\theta d\varphi^2$, from the TOV equations given in (2) and (3) one can easily obtain:

$$\frac{d\phi}{dp} = -\frac{1}{p}, \quad (5)$$

and the solution of this equation is $p = p_0 e^{-\phi(r)}$, where p_0 is the integration (aether pressure) constant. In general relativity, the pressure of gravitational fields is not inherently negative. The curvature of spacetime is influenced by the distribution of matter and energy. The properties of the gravitational field, such as pressure and energy density, are determined by the stress–energy tensor, which describes the matter and energy content of the system. In typical situations, the pressure associated with gravitational fields can be positive, negative, or even zero, depending on the distribution and nature of the matter and energy sources involved. For example, in the case of ordinary matter, the pressure is typically positive. However, there are certain exotic forms of matter or energy, such as dark energy or certain hypothetical fields, where the pressure may be negative. If the aether exists in nature, it must be a shear-free tensile material with a constant tension equal to its energy density. However, no known material of this nature currently exists. Nevertheless, it is still worth considering the theoretical possibility. Einstein’s introduction of a positive cosmological constant in their gravitational field equations, dating back to 1915, is equivalent to assuming that the Universe is filled with an ideal fluid exhibiting negative pressure equal to its constant energy density. This form of “dark energy” can also be conceived as a tensile material with a tension of Λ that adheres to local Lorentz invariance. Consequently, dark energy can be considered to be a type of aether. Therefore, this negative pressure can lead to phenomena such as the accelerated expansion of the Universe.

Equation (5) corresponds to the condition of hydrostatic equilibrium governing the aether field. This condition remains applicable regardless of assuming spherical symmetry, being valid for any static spacetime.

If one integrates Equation (6) by using Equation (5)

$$\frac{d\phi}{dr} = \frac{M + 4\pi r^3 p_0 e^{-\phi(r)}}{r(r - 2M)}, \quad (6)$$

The equation at hand can be solved by recognizing it as a first-order inhomogeneous linear differential equation in $e^{\phi(r)}$, and the solution is given in [4] as:

$$e^{\phi(r)} = \sqrt{1 - \frac{2M}{r}} (1 + 4\pi p_0 f(r)), \quad (7)$$

with

$$f(r) = \frac{r^2}{2} \left(1 - \frac{2M}{r}\right)^{-\frac{1}{2}} \left(1 + \frac{5M}{r} - \frac{30M^2}{r^2}\right) + \frac{15}{2} M^2 \ln \left[\frac{r}{M} \left(1 + \sqrt{1 - \frac{2M}{r}}\right) - 1 \right] \quad (8)$$

From the metric (4), we can see that the horizon of this spacetime is located at $r_h = 2M$, and it is solely dependent on the mass of the black hole without any dependence on other parameters of the spacetime.

3. Scalar Invariants

The expression of the scalar invariants such as the Ricci scalar, the square of Ricci tensor, and Kretschmann scalars for the spacetime given in Equation (4) are calculated in the next subsections.

3.1. Ricci Scalar

The Ricci scalar, also known as the scalar curvature, is a fundamental curvature invariant in curved spacetime. It is defined as $R = g^{\mu\nu} R_{\mu\nu}$, where $R_{\mu\nu}$ represents the Ricci tensor. Positive and negative values of the Ricci scalar correspond to a sunken and convex curvature of spacetime, respectively. By performing straightforward mathematical calculations, one can readily obtain the expression for the Ricci scalar.

$$\mathcal{R} = g^{\mu\nu} R_{\mu\nu} = -\frac{8\pi p_0}{r(4\pi p_0 f(r) + 1)} \left\{ \left(2 - \frac{M}{r}\right) f'(r) - r \left(1 - \frac{2M}{r}\right) f''(r) \right\}. \quad (9)$$

3.2. Square of Ricci Tensor

Let us consider the second scalar invariant known as the square of the Ricci tensor. This invariant is associated with the square of the energy–momentum tensor of a field in the spacetime of a black hole (BH). It is defined as $\mathcal{R} = R_{\mu\nu} R^{\mu\nu} \equiv 1/(8\pi G) T_{\mu\nu} T^{\mu\nu}$ for the spacetime around the aether black holes (4). The expression for the square of the Ricci tensor is given by:

$$R_{\mu\nu} R^{\mu\nu} = \frac{32\pi^2 p_0^2}{(1 + 4\pi p_0 f(r))^2} \left\{ \left(1 - \frac{2M}{r}\right)^2 f''(r)^2 + \frac{3}{r^2} f'(r)^2 \right. \\ \left. \times \left(1 - \frac{2M}{r} + \frac{3M^2}{r^2}\right) + \frac{2}{r} \left(1 + \frac{M}{r}\right) \left(1 - \frac{2M}{r}\right) f'(r) f''(r) \right\} \quad (10)$$

3.3. Kretschmann Scalar

Next, we turn our attention to the Kretschmann scalar, denoted as $\mathcal{K} = R_{\mu\nu\sigma\rho} R^{\mu\nu\sigma\rho}$. The square root of the Kretschmann scalar is often associated with an effective gravitational energy density, represented as $\sqrt{\mathcal{K}} \sim \rho_M$. We can straightforwardly compute the Kretschmann scalar for the spacetime metric (4) as follows:

$$\begin{aligned}
\mathcal{K} = R^{\mu\nu\alpha\beta}R_{\mu\nu\alpha\beta} = & \frac{16}{r^6(4\pi p_0 f(r) + 1)^2} \left\{ 3M^2 + 4\pi p_0 r \left[\pi p_0 r^5 \left(1 - \frac{2M}{r} \right)^2 f''(r)^2 \right. \right. \\
& + \pi p_0 r^3 \left(2 - \frac{8M}{r} + \frac{17M^2}{r^2} \right) f'(r)^2 + Mr \left(1 - \frac{5M}{r} \right) f'(r) - Mr^2 \left(1 - \frac{2M}{r} \right) f''(r) \\
& \left. \left. (1 - 6\pi p_0 r f'(r)) + Mf(r) \left[4\pi p_0 r \left\{ \left(1 - \frac{5M}{r} \right) f'(r) - r \left(1 - \frac{2M}{r} \right) f''(r) \right\} + \frac{6M}{r} \right] \right. \right. \\
& \left. \left. + 48\pi M^2 p_0 f(r)^2 \right\} \right\} \quad (11)
\end{aligned}$$

Figure 1 presents the radial variations of scalar invariants in the spacetime (4), including the Ricci scalar (top left panel), the square of Ricci tensor (top right panel), and the Kretschmann scalar (bottom panel) for various values of the pressure parameter p_0 . The figure illustrates that the scalar invariants exhibit a decreasing trend along the radial coordinates. Additionally, as the absolute value of p_0 increases, the scalar invariants also experience an increase.

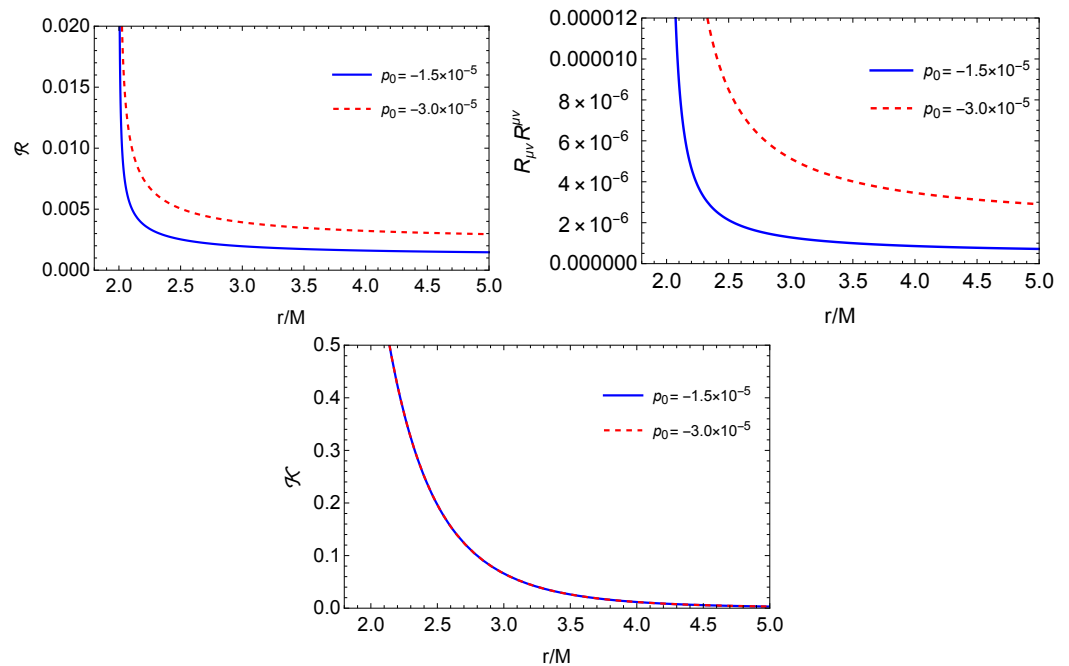


Figure 1. Radial dependence of Ricci scalar (top left panel), the square of Ricci tensor (top right panel), and Kretschmann scalar (bottom panel) for different values of the pressure parameter p_0 .

4. Motion of a Test Particle in the Vicinity of the Aether BH

In this section, we explore the circular orbit of test particles with mass m around a black hole in the context of gravitational aether by employing the Hamilton–Jacobi equation.

$$g^{\mu\nu} \frac{\partial S}{\partial x^\mu} \frac{\partial S}{\partial x^\nu} = -m^2, \quad (12)$$

We derive the equation of motion using a separable form of the action S as,

$$S = -Et + L\varphi + S_r + S_\theta, \quad (13)$$

where E and L are energy and the angular momentum of the test particle, acting as the conserved quantities of the motion.

After inserting it into Equation (12) and separating the variables in the equation, we arrive at the radial motion equation in the equatorial plane $\theta = \pi/2$ as follows:

$$(1 + 4\pi p_0 f(r))^2 \left(\frac{dr}{d\tau} \right)^2 = \mathcal{E}^2 - V_{\text{eff}} \quad (14)$$

Here, τ represents the proper time along the particle's trajectory, and the effective potential for radial motion is given by:

$$V_{\text{eff}}(r, \mathcal{L}, p_0) = \left(1 + 4\pi p_0 f(r)\right)^2 \left(1 - \frac{2M}{r}\right) \left(1 + \frac{\mathcal{L}^2}{r^2}\right) \quad (15)$$

In the above expressions, we have replaced E/m with \mathcal{E} and L/m with \mathcal{L} . Notably, the effective potential depends not only on the energy, angular momentum, and the radius of motion but also on the aether pressure p_0 .

In Figure 2, the radial dependence of the effective potential of the radial motion of the test particle around gravitational aether BH (for different values of the aether pressure p_0) is observed graphically. For comparison, we have also plotted the Schwarzschild dependence, corresponding to $p_0 = 0$. We can see that the effective potential in the presence of gravitational aether exhibits higher values compared to the case of Schwarzschild, represented by the dashed red line. It is also observed that the aether field effects on the effective potential are significant at large distances from the central BH. One can easily see that the orbits of the particles become more stable with increasing modules of p_0 .

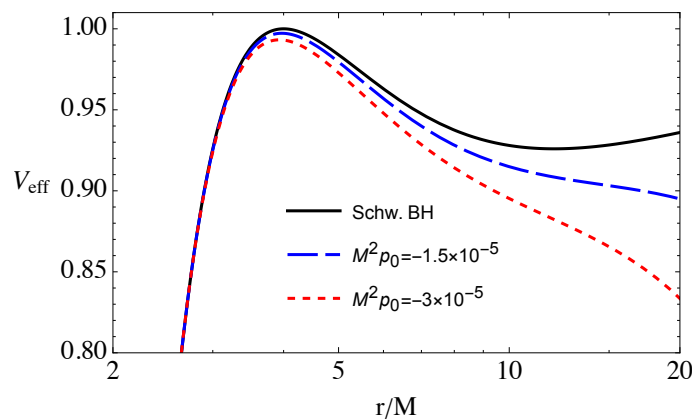


Figure 2. Radial dependence of the effective potential of the radial motion of the test particles around a BH in the gravitational aether theory for different values of the pressure p_0 . Here, we chose the angular momentum of the particle as $\mathcal{L} = 4.3M$.

The specific angular momentum of test particles along the circular motion can be obtained by solving the equation $\partial_r V_{\text{eff}}(r) = 0$, given as:

$$\mathcal{L}^2 = \frac{r^2(4\pi p_0 r(r-2M)f'(r) + M[1 + 4\pi p_0 f(r)])}{(r-3M)[1 + 4\pi p_0 f(r)] - 4\pi p_0 r(r-2M)f'(r)} \quad (16)$$

and the energy

$$\mathcal{E}^2 = \frac{(r-2M)^2[1 + 4\pi p_0 f(r)]^3}{r[(r-3M)[1 + 4\pi p_0 f(r)] - 4\pi p_0 r(r-2M)f'(r)]} \quad (17)$$

Figure 3 illustrates the radial dependencies of the specific energy and angular momentum for particles in circular orbits around a black hole in the gravitational aether, considering various values of p_0 , along with a comparison of the Schwarzschild limit

($p_0 = 0$). From the plot, it is evident that both the energy and the angular momentum decrease as the absolute value of p_0 increases.

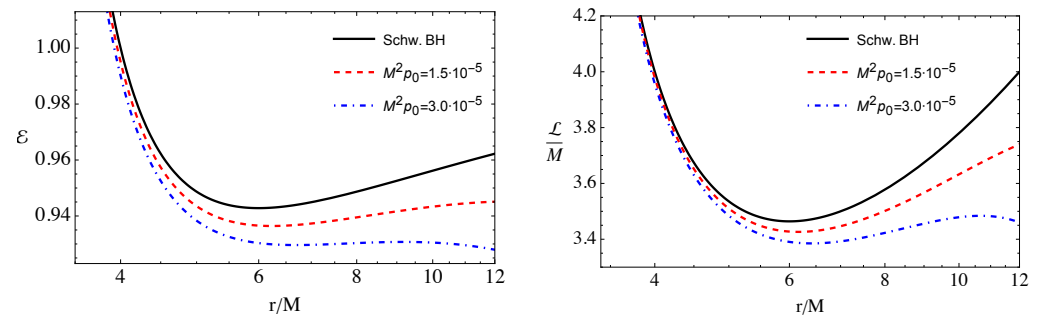


Figure 3. Radial dependence of energy and angular momentum of the particle in the circular orbits around a black hole in gravitational aether for the different values of the p_0 . For comparison, we have also plotted the Schwarzschild BH case, corresponding to $p_0 = 0$.

In Figure 4, the energy \mathcal{E} and angular momentum \mathcal{L} of the test particle moving radially around the BH have been studied graphically. Note that the particle orbiting in the Schwarzschild geometry has higher values of energy and angular momentum compared to the case when the aether parameter $p_0 \neq 0$ is present. It is observed that as the value of p_0 increases, the energy and angular momentum decrease, and this behavior is more prominent as the particle moves away from the central object.

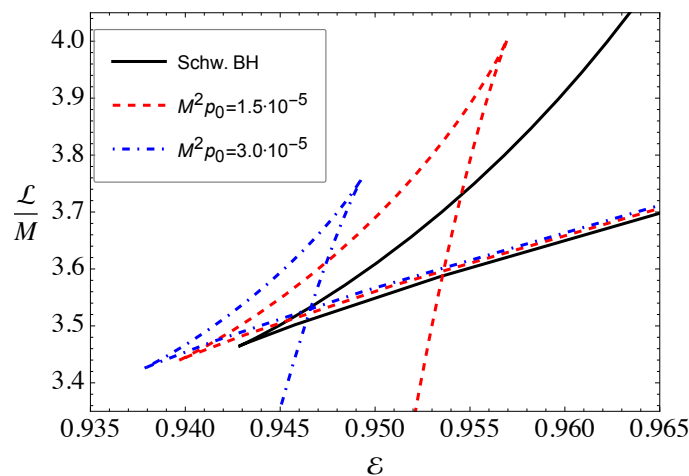


Figure 4. Relationships between angular momentum and energy of test particles corresponding to circular orbits around gravitational aether black hole for different values of p_0 .

$$\begin{aligned}
 & 2p \left\{ (r) (pr(r-2M)(r(2M-r)f''(r) + (10M-3r)f'(r)) + 4M(6M-r)) \right. \\
 & \left. + r(r-2M)(f'(r)(2pr(r-2M)f'(r) + 10M-3r) - r(r-2M)f''(r)) \right. \\
 & \left. + 2Mpf(r)^2(6M-r) \right\} + 4M(6M-r) = 0
 \end{aligned} \quad (18)$$

Because Equation (18) has a complex form that cannot be solved analytically to obtain the ISCO radius, we performed graphical analyses of the ISCO radius in Figure 5.

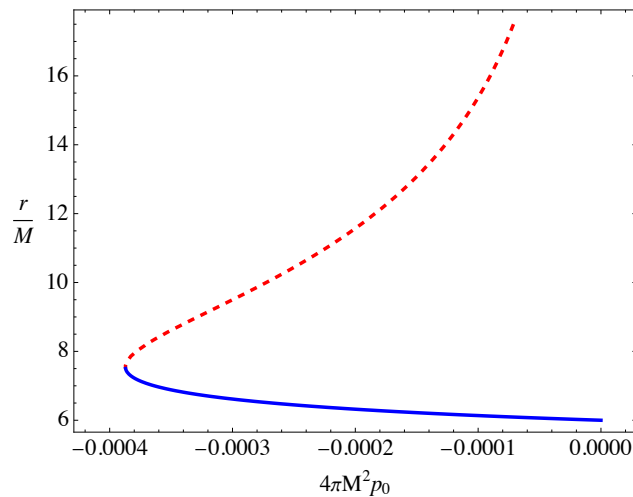


Figure 5. Dependence of the radius of the ISCOs (r_{ISCO} in solid blue line) and OSCOs (r_{OSCO} in red dashed line) on p_0 .

In Figure 5, we have shown the radius of ISCO as a function of p_0 . It is shown that an increase in p_0 causes a decrease in the ISCO radius and, at the Schwarzschild limit $p_0 = 0$, the ISCO radius equals $6M$ (as expected). Furthermore, upon solving Equation (18), two real solutions for r are obtained for each value of negative p_0 , one of which is greater than the other corresponding ISCO (solid blue) and outermost circular stable orbits (OSCO) (red dashed), respectively. Since the smaller solution corresponds to the ISCO, we consider the smaller solution. As p_0 approaches the critical value $\pi M^2 p_0 \simeq -10^{-4}$, Equation (18) yields a single solution for the radius, indicating that this is the smallest value of p_0 where ISCO and OSCO coincide each other. For values of p_0 smaller than this critical value, there are no real solutions for the radius, implying the absence of an ISCO.

In fact, a way of determining the types of black hole in astrophysical observations is to measure their ISCO radius, the inner radius of accreting matter around the black hole. In this sense, the effects of the aether field parameter and negative spin parameter of rotating Kerr black holes are similar: the presence of both parameters causes increasing the ISCO radius showing degeneracy effects. Here, we find degeneracy values of the spin of the Kerr black hole and the aether parameters using the numerical solution of Equation (18).

Figure 6 shows relationships between the values of spin of rotating Kerr black holes and the pressure parameter of gravitational aether, which provide the same ISCO radius. Moreover, our performed analysis reveals that as the parameter p_0 becomes available, to preserve the same ISCO radius, the Kerr parameter must be about $0.4M$ and an increase in the absolute value of the pressure p_0 leads to a decrease in the Kerr spin parameter.

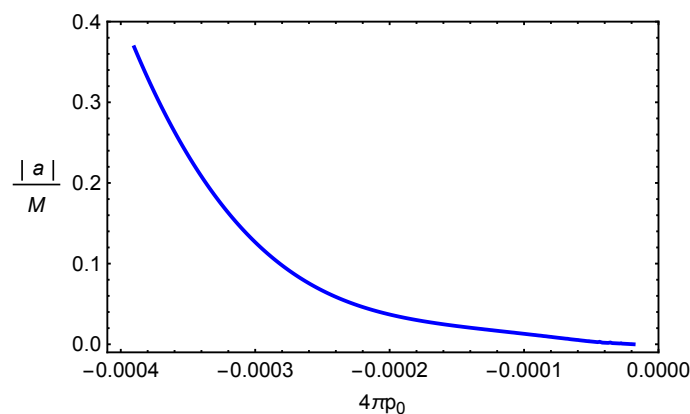


Figure 6. The degeneracy graphs between the spin $|a|$ and the aether pressure p_0 providing the same ISCO radius for the different values of p_0 .

5. The Efficiency of Energy Extraction

The accretion process around a black hole involves particles moving in Keplerian orbits, and the Novikov–Thorne model is often employed to describe the geometrically thin accretion disk. According to this model, the efficiency of energy extraction from the accretion disk can be calculated as the difference between the energy of matter falling into the black hole from the disk at the ISCO and its rest mass energy. This extracted energy is assumed to be converted into electromagnetic radiation, contributing to the total bolometric luminosity of the accretion disk. The energy efficiency, denoted as η , can be expressed as the ratio of the bolometric luminosity (L_{bol}) to the rest mass energy accretion rate ($\dot{M}c^2$) from the disk [39]. In this context, the efficiency of the accretion process is evaluated.

$$\eta = 1 - \mathcal{E}_{\text{ISCO}}, \quad (19)$$

where $\mathcal{E}_{\text{ISCO}}$ is the energy of the particle at ISCO, $r = r_{\text{ISCO}}$, and it is calculated using the energy of the particles given by Equation (17) at ISCO.

The influence of the aether parameter p_0 on the efficiency of test particle accretion around black holes in aether gravity is depicted in Figure 7. It is evident from the graph that the efficiency increases almost linearly as the absolute value of the aether parameter rises, reaching a peak of approximately $\eta \approx 14.2\%$ within the range of the parameter $p_0 = (-p_{\text{cr}}, 0)$. However, in fact, the aether parameter can mimic the spin of rotating Kerr black holes providing the same efficiency in measurements of the total bolometric luminosity of a black hole accretion disk. Now, we show how the aether field mimics the spin parameter in terms of the same luminosity.

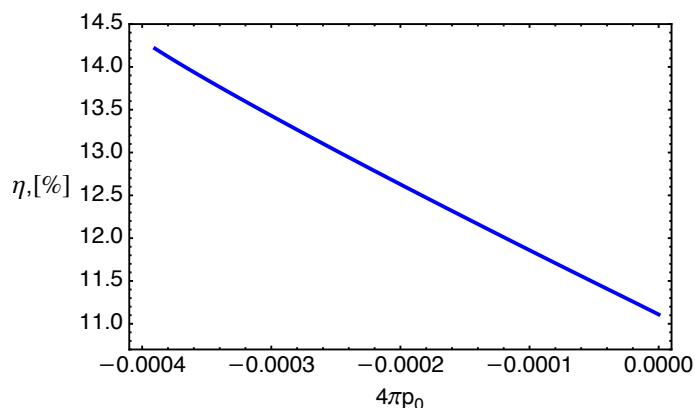


Figure 7. Dependence of energy efficiency from the aether pressure p_0 for the different values of p_0 . The maximal efficiency is at about critical pressure $4\pi M^2 p_{\text{cr}} = -4 \times 10^{-4}$.

In Figure 8, we have shown the efficiency of energy release from particles in corotating and contour rotating orbits around Kerr black holes. It is observed that in the corotating case, the efficiency increases exponentially with the spin parameter increase and reaches up to about 42%. However, in the contour rotating case, the efficiency increases first and reaches its maximum at about 5.9% up to about $a \simeq 0.2M$ and then as the spin parameter increases the efficiency decreases back up to about 5.2%.

The mimicking values between the spin parameter and the aether pressure p_0 provide the same energy efficiency.

Figure 9 illustrates the degeneracy between the spin parameter of a rotating Kerr black hole a and the pressure parameter of the gravitating aether field p_0 in terms of the same value in the energy efficiency. It can be observed that with an increase in the aether pressure parameter, the Kerr spin parameter should decrease to maintain a constant energy efficiency level.

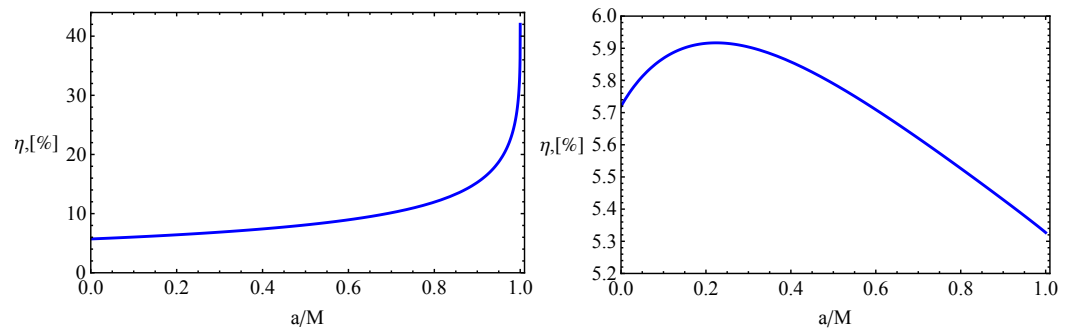


Figure 8. The efficiency of energy release from corotating and contour rotating test particles around the Kerr black hole.

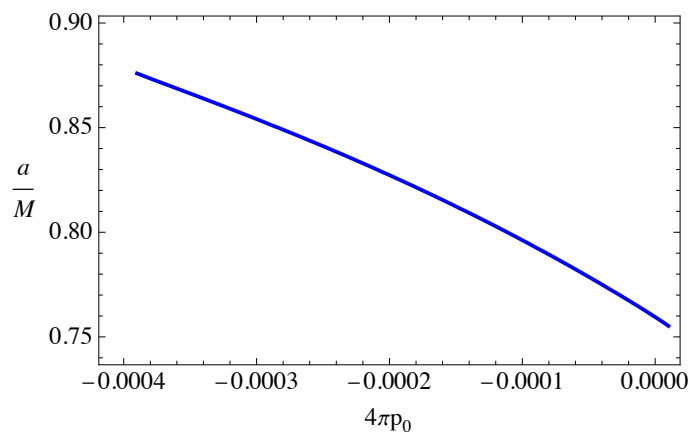


Figure 9. The degeneracy graphs between the spin parameter and the aether pressure p_0 that provide the same energy efficiency.

6. Center of Mass Energy of the Colliding Particles

For the first time, Banados–Silk–West (BSW) proposed a theoretical analysis of the process of high-energy particle collisions close to the black hole horizon, which might be a source of energy extraction from the black hole. Subsequent research has been conducted in various contexts to expand upon this work, and it has been established that head-on collisions are more successful in extracting energy from the central black hole.

In this section, we analyze the collision of neutral particles in a gravitational aether black hole spacetime, and the associated radial velocity and critical angular momentum of these particles, originating from infinity. The center of mass of the colliding particles can be determined using the following relation.

$$\begin{aligned} \frac{E_{cm}^2}{2m^2} &= 1 - g_{\mu\nu}u_1^\mu u_2^\nu \\ &= 1 - g_{tt}\dot{t}_1\dot{t}_2 - g_{rr}\dot{r}_1\dot{r}_2 - g_{\varphi\varphi}\dot{\varphi}_1\dot{\varphi}_2 \end{aligned} \quad (20)$$

The constants of motion can be found from Equation (13) in the following way:

$$g_{tt}\dot{t} = -\mathcal{E}, \quad g_{\varphi\varphi}\dot{\varphi} = \mathcal{L} \quad (21)$$

and we can obtain radial velocity from Equation (14):

$$\dot{r}^2 = \frac{\mathcal{E}^2}{(1 + 4\pi p_0 f(r))^2} - \left(1 - \frac{2M}{r}\right) \left(1 + \frac{\mathcal{L}^2}{r^2}\right) \quad (22)$$

Utilizing the above equations, the expression for the center of mass energy of the colliding particles can be derived as follows:

$$\frac{E_{cm}^2}{2m^2} = 1 - \frac{\mathcal{E}_1 \mathcal{E}_2}{g_{tt}} - \frac{\mathcal{L}_1 \mathcal{L}_2}{g_{\varphi\varphi}} - g_{rr} \sqrt{\frac{\mathcal{E}_1^2}{(1 + 4\pi p_0 f(r))^2} - \left(1 - \frac{2M}{r}\right) \left(1 + \frac{\mathcal{L}_1^2}{r^2}\right)} \quad (23)$$

$$\times \sqrt{\frac{\mathcal{E}_2^2}{(1 + 4\pi p_0 f(r))^2} - \left(1 - \frac{2M}{r}\right) \left(1 + \frac{\mathcal{L}_2^2}{r^2}\right)}$$

The critical angular momentum of the particles is an essential parameter for particles coming from infinity, as it denotes the limit in the angular momentum of the particles; if the particle's angular momentum exceeds the critical value, it cannot approach the central object. To obtain the critical angular momentum value, conditions $\dot{r}^2 = 0$ and $d\dot{r}^2/dr = 0$ must be satisfied.

The square of the radial velocity, as seen in Figure 10, becomes negative for certain values of the angular momentum, indicating that if the angular momentum is greater than the critical value, the particle cannot come close to the black hole, as the radial velocity is negative.

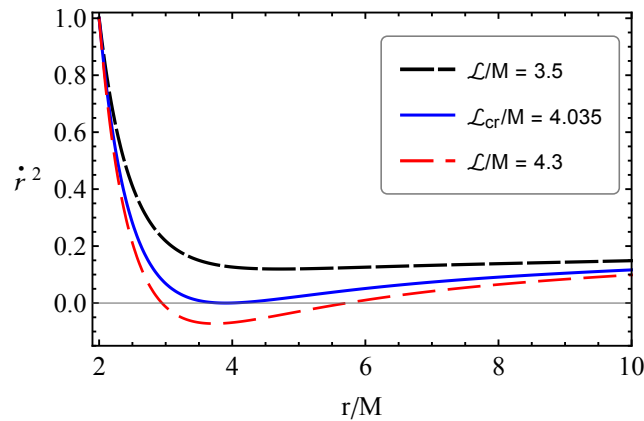


Figure 10. The dependence of the square of the radial velocity to the radial distance in different values of angular momentum $4\pi p_0 = -0.0003$.

Figure 11 shows the dependence of the critical angular momentum on the aether constant $4\pi p_0$. It can be seen that the critical angular momentum is linearly proportional to the aether pressure constant. For the given values of the aether pressure constant, the angular momentum ranges between $\mathcal{L}_{cr} = 4.0 \sim 4.05$.

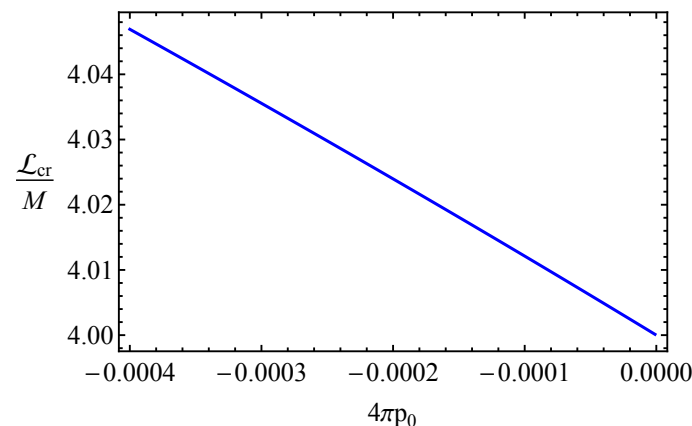


Figure 11. The dependence of the critical angular momentum to $4\pi p_0$.

Figure 12 shows the radial dependence of the center of mass energy of two colliding particles with the angular momentum $\mathcal{L}/M = \pm 4$ and ± 2 at left and right panels, respectively. It can be seen that the aether pressure constant does not have a significant effect, but there is a difference near the horizon.

The right panel of this figure shows the colliding particles with a critical angular momentum value, as described in the following subsection.

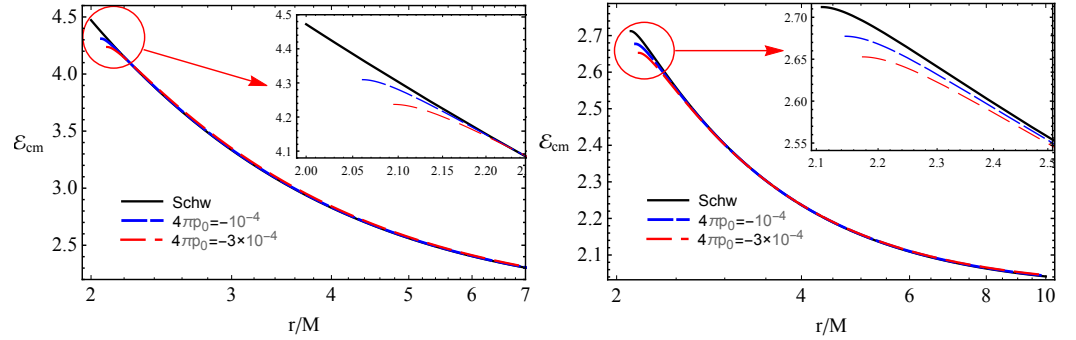


Figure 12. Radial dependence of the center of mass energy of two colliding particles with angular momentum $\mathcal{L}_1 = -\mathcal{L}_2 = 4$ (left panel) and $\mathcal{L}_1 = -\mathcal{L}_2 = 2$ (right panel).

7. Fundamental Frequencies

In this section, we calculate the fundamental frequencies of test particles moving in circular orbits around the black hole with a gravitational aether. This serves as a simplified model for explaining the presence of QPOs observed around black holes.

7.1. Keplerian Frequency

The angular velocity of the test particle around the gravitational aether black hole, as measured by a distant observer, commonly referred to as the Keplerian frequency, can be expressed as follows:

$$\Omega_K^2 = \frac{M}{r^3} + p_0 \frac{r(r-2M)f'(r) + 2Mf(r)}{2r^3}, \quad (24)$$

To obtain the values of the fundamental frequencies in units of Hz, one can multiply the frequencies by the factor $c^3/(2\pi GM)$. Here, we employ the values for the speed of light in a vacuum, $c = 3 \times 10^8$ m/s, and the gravitational constant, $G = 6.67 \times 10^{-11}$ m³/(kg² · s).

7.2. Harmonic Oscillations

When a test particle is in a stable circular orbit at the equatorial plane around the black hole, small perturbations in its radial ($r \rightarrow r_0 + \delta r$) and vertical ($\theta \rightarrow \theta_0 + \delta \theta$) coordinates cause oscillations along these axes.

To derive the equations that govern these oscillations, we expand the effective potential in terms of the coordinates r and θ and use the conditions for the extrema of the effective potential, namely $V_{\text{eff}}(r_0, \theta_0) = 0$ and $\partial_{r(\theta)} V_{\text{eff}} = 0$. This leads to the following expressions:

$$\frac{d^2 \delta r}{dt^2} + \Omega_r^2 \delta r = 0, \quad \frac{d^2 \delta \theta}{dt^2} + \Omega_\theta^2 \delta \theta = 0, \quad (25)$$

Here, Ω_r^2 and Ω_θ^2 represent the square of the radial and vertical angular frequencies of the particles around the black hole, respectively, as measured by a distant observer. They are given by:

$$\Omega_r^2 = -\frac{1}{2g_{rr}(u^t)^2} \partial_r^2 V_{\text{eff}}(r, \theta) \Big|_{\theta=\pi/2}, \quad (26)$$

$$\Omega_{\theta}^2 = -\frac{1}{2g_{\theta\theta}(u^t)^2} \partial_{\theta}^2 V_{\text{eff}}(r, \theta) \Big|_{\theta=\pi/2}, \quad (27)$$

After performing some algebraic calculations, we obtain the expressions for the radial and vertical frequencies as follows:

$$\begin{aligned} \Omega_r^2 &= \frac{1}{4r^4} \left\{ 2p_0 \left[f(r)(p_0 r(r-2M)(r-2M)f''(r) + (3r-10M)f'(r)) + 4M(r-6M) \right] \right. \\ &+ r(r-2M)(r-2M)f''(r) + f'(r)(2p_0 r(2M-r)f'(r) - 10M + 3r) \\ &\left. + 2Mp_0 f(r)^2(r-6M) \right] + 4M(r-6M) \Big\}, \end{aligned} \quad (28)$$

$$\Omega_{\theta} = \Omega_{\phi} = \Omega_K \quad (29)$$

Additionally, Figure 13 presents the radial dependence of the Keplerian frequencies of test particles around gravitational aether black holes.

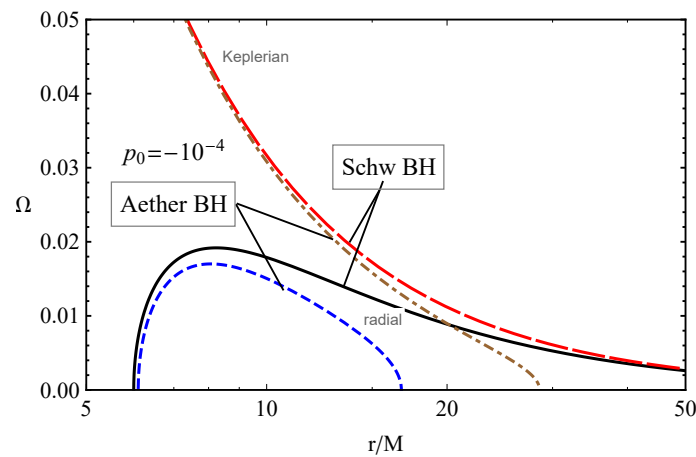


Figure 13. Keplerian frequencies (red large dashed line and brown dot dashed line) and the frequency of radial oscillations (solid black and blue dashed lines) of test particles around gravitational aether black holes as a function of radial coordinates.

Figure 13 illustrates the radial dependence of the frequency of particle oscillations in the radial, vertical, and angular directions. A comparison with the Schwarzschild case reveals that in the presence of the aether pressure p_0 , the frequencies slightly decrease compared to the Schwarzschild scenario. Moreover, it is also observed that the presence of p_0 restricts the range of radial distances where the frequencies occur, with radial oscillation frequencies limited to approximately $r \in (6M, 17M)$ where a closer one corresponds to ISCO and the other is for OSCO. Similarly, there are angular oscillation frequencies up to $r \approx 30M$.

8. QPOs

Black holes do not emit electromagnetic information about their surface, but they play a significant role in the radiation processes that occur in the accretion disk. QPOs are astrophysical phenomena observed in Fourier analyses of the continuous electromagnetic radiation emitted by the accretion disk surrounding a black hole. The source of electromagnetic emission in the accretion disk is closely linked to the oscillations of particles. When a charged particle oscillates, it emits an electromagnetic wave with a frequency equal to its oscillation frequency. Therefore, the dynamics of charged test particles around black holes can explain the origin of QPOs through their oscillations in the radial and angular directions. Various QPO models have been proposed and developed to explain different sources of QPOs. In this study, we consider the following models:

- Relativistic Precession (RP) model: Originally introduced in Ref. [29] to explain the kHz twin-peak QPOs observed in neutron stars of Low-Mass X-ray Binary systems. Later, the RP model was shown to be applicable to black hole candidates in binary systems involving black holes and neutron stars [40]. The RP model was further developed in Ref. [41] to obtain mass and spin measurements of black holes located at the centers of microquasars, utilizing data from the power-density spectrum of the accretion disk. In the RP model, the upper and lower frequencies are described by the frequencies of the fundamental oscillations, $\nu_U = \nu_\phi$ and $\nu_L = \nu_\phi - \nu_r$, respectively.
- Epicyclic resonance (ER) model: This model is based on the resonances of modes of axisymmetric oscillations in the accretion disk of black holes [42]. It has been demonstrated that the oscillation modes of the disk are related to the frequencies of harmonic (quasi-) oscillations of circular geodesics of test particles. We consider two submodels within the ER model: ER2 and ER3, which differ in their oscillation modes. The upper and lower frequencies in the ER2 and ER3 models are given by $\nu_U = 2\nu_\theta - \nu_r$ and $\nu_L = \nu_r$, and $\nu_U = \nu_\theta + \nu_r$ and $\nu_L = \nu_\theta - \nu_r$, respectively, [42].
- Warped Disc (WD) model: This model utilizes the nonaxisymmetric oscillatory modes of the accretion disk oscillations around black holes and neutron stars [43,44]. According to the WD model, the upper and lower frequencies are $\nu_U = 2\nu_\phi - \nu_r$ and $\nu_L = 2(\nu_\phi - \nu_r)$, respectively, and the vertical oscillations cause the thin accretion disk to warp [43,44].

We proceed by analyzing the possible values of the upper and lower frequencies of twin-peaked QPOs generated by the oscillating particles along their stable circular orbits around a black hole in the gravitational aether field using the aforementioned models and present the results graphically.

Figure 14 depicts the relationships between the upper and lower frequencies of twin-peak QPOs corresponding to different models of black holes and QPO sources. In our numerical calculations, we consider black holes with a mass of $5M_\odot$, representing stellar-mass black holes. The figure reveals several key observations. Firstly, an increase in the absolute value of the pressure parameter leads to a decrease in the possible values of the frequency ratio. Additionally, it is notable that QPOs are not observed in the low-frequency regime. Furthermore, the figure demonstrates that the pressure parameter cannot emulate the spin of a Kerr black hole, as it fails to provide identical values for the upper and lower frequencies in twin-peaked QPOs.

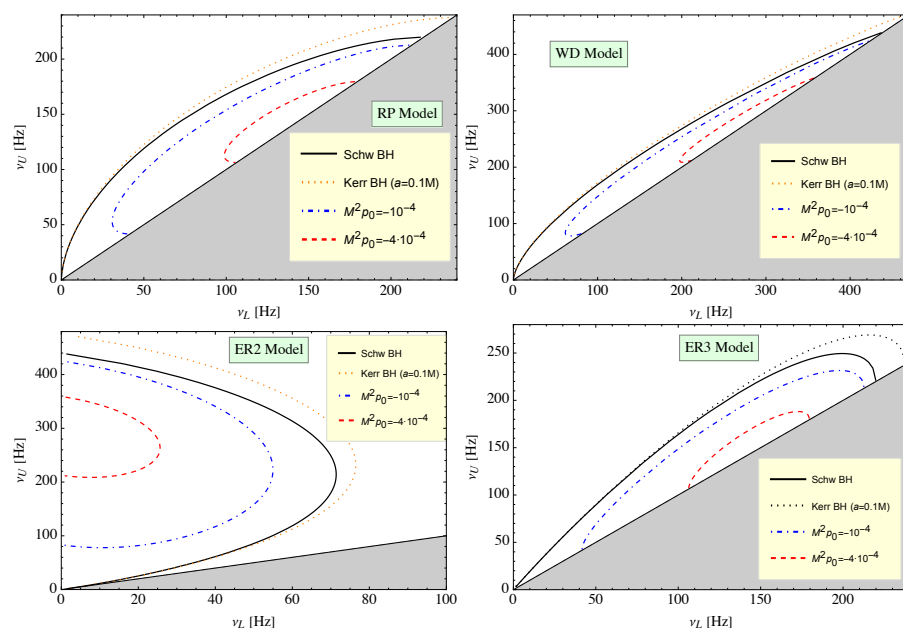


Figure 14. Cont.

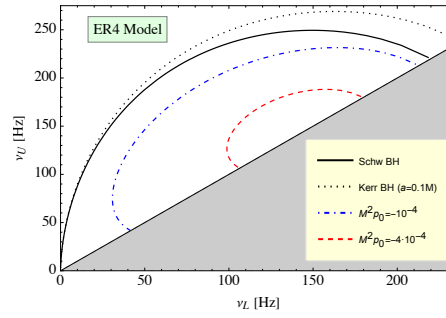


Figure 14. Relations between the frequencies of upper and lower picks of twin-pick QPOs in the RP, WD, and ER2-4 models around an aether black hole.

9. Constraints on the BH Mass and Aether Parameter

In this section, we aim to obtain constraints on the values of the pressure parameter of the gravitational field surrounding the Schwarzschild black hole and its mass using frequencies of the QPOs from the microquasars GRO J1655-40 and GRS 1915+105. According to the relativistic precession model, the frequencies of the periastron precession ν_{per} and the nodal precession ν_{nod} are defined by the following relations: $\nu_{\text{per}} = \nu_{\phi} - \nu_r$ and $\nu_{\text{nod}} = \nu_{\phi} - \nu_{\theta}$, respectively, [35,45].

In order to obtain the estimation for the five parameters as the peak frequencies of QPOs observed in the microquasars, we perform the χ^2 analysis with [46]

$$\begin{aligned} \chi^2(M, B, r_1, r_2) = & \frac{(\nu_{1\phi} - \nu_{1U})^2}{\sigma_{1U}^2} + \frac{(\nu_{1\text{per}} - \nu_{1L})^2}{\sigma_{1L}^2} \\ & + \frac{(\nu_{1\text{nod}} - \nu_{1C})^2}{\sigma_{1C}^2} + \frac{(\nu_{2\phi} - \nu_{2U})^2}{\sigma_{2U}^2} \\ & + \frac{(\nu_{2\text{nod}} - \nu_{2C})^2}{\sigma_{2C}^2} . \end{aligned} \quad (30)$$

In fact, the best estimates for the values of the parameters M , p , r_1 , and r_2 that make χ_{min}^2 to be minimum and the range of the parameters at the confidence level (C.L.) can be determined in the interval $\chi_{\text{min}}^2 \pm \Delta\chi^2$.

9.1. GRO J1655-40

Here, we obtain constraints on the mass of the black hole and surrounding aether field pressure in the microquasar GRO J1655-40 using the two sets of QPO frequencies in the astrophysical observations [27],

$$\begin{aligned} \nu_{1U} &= 441 \text{ Hz}, & \sigma_{1U} &= 2 \text{ Hz}, \\ \nu_{1L} &= 298 \text{ Hz}, & \sigma_{1L} &= 4 \text{ Hz}, \\ \nu_{1C} &= 17.3 \text{ Hz}, & \sigma_{1C} &= 0.1 \text{ Hz} \end{aligned} \quad (31)$$

and

$$\begin{aligned} \nu_{2U} &= 451 \text{ Hz}, & \sigma_{2U} &= 5 \text{ Hz}, \\ \nu_{2C} &= 18.3 \text{ Hz}, & \sigma_{2C} &= 0.1 \text{ Hz} . \end{aligned} \quad (32)$$

It is obtained that the χ^2 take minimum as $\chi_{\text{min}}^2 = 0.000129108$ at $r_1 = 6.9069M$, $r_2 = 9.4529M$, $M = 16.1843M_{\odot}$, $p_0 = -0.0756$.

9.2. GRS 1915+105

Furthermore, we perform a similar analysis on the GRS 1915+105 microquasar with QPO frequencies [47],

$$\begin{aligned} \nu_{1U} &= 184.10 \text{ Hz}, & \sigma_{1U} &= 1.84 \text{ Hz}, \\ \nu_{2U} &= 142.98 \text{ Hz}, & \sigma_{2U} &= 3.48 \text{ Hz}, \end{aligned} \quad (33)$$

and

$$\begin{aligned} \nu_{1L} &= 67.40 \text{ Hz}, & \sigma_{1L} &= 0.60 \text{ Hz}, \\ \nu_{2L} &= 65.89 \text{ Hz}, & \sigma_{2L} &= 0.52 \text{ Hz}, \\ \nu_{3L} &= 69.58 \text{ Hz}, & \sigma_{3L} &= 0.49 \text{ Hz}. \end{aligned} \quad (34)$$

and it is also found that $\chi_{min}^2 = 9.1966 \times 10^{-15}$ at the best fit values of the parameters $r_1 = 7.11812M$, $r_2 = 9.525M$, $p = -0.0956658$, and $M = 44.4246M_\odot$.

In Figure 15, the best values of the pressure of the aether field p and the mass of the central black hole in the center of GRO J1655-40 (left panel) and GRS 1915+105 (right panel). Furthermore, we present the contour levels 1σ , 2σ , and 3σ of p and M/M_\odot .

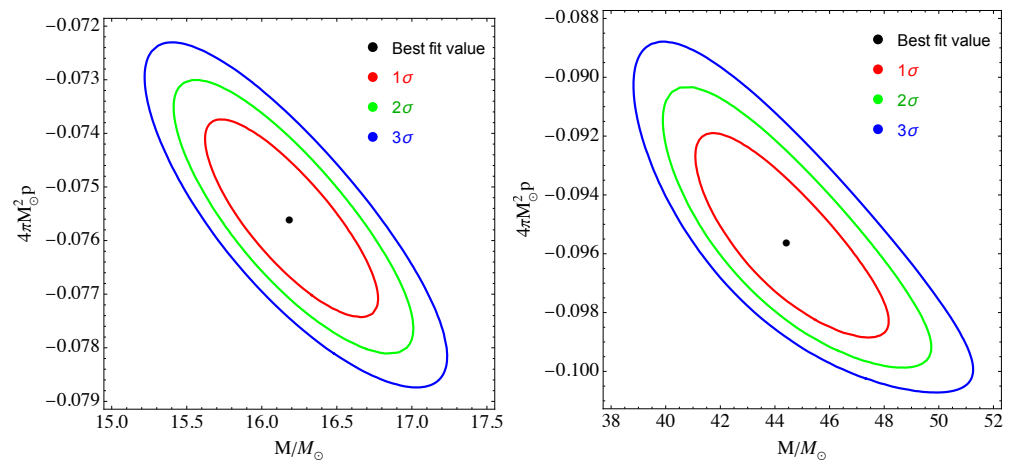


Figure 15. Constraints on black hole mass and the aether pressure in the microquasars GRO J1655-40 (left panel) and GRS 1915+105 (right panel).

10. Conclusions

In the present work, we have studied test particle motion around a black hole surrounded by a gravitational aether field. The results obtained can be summarized as follows:

- First, we have explored the spacetime structure by analyzing the scalar invariants. It has been shown that the presence of the aether field causes a decrease in the Ricci scalar and the square of the Ricci tensor. We have also shown that the Kretschmann scalar is less sensitive to the change in aether parameter.
- We performed an analysis of the dynamics of test particles around the black hole in the presence of aether. Particularly, we explored the circular orbits of the particles around the central object. The study of specific energy and angular momentum of test particles corresponding to circular orbits around the black hole has shown that both energy and angular momentum decrease in the presence of the aether field. However, the ISCO radius increases with increasing absolute values of the aether parameter.
- Collisions of test particles near the aether black holes have also been studied. The critical value of the angular momentum of the colliding particle, in which collision may occur, has been analyzed. Our analysis has shown that in the presence of the aether field, the angular momentum increases slightly and takes values between $\mathcal{L}_{cr}/M \in (4.05 \div 0)$ and the corresponding values of $4\pi M^2 p \in -4 \times 10^{-4} \div 0$. The expression for the center of mass energy has been obtained, and it has been shown that the latter decreases with the increase in the absolute value of the aether parameter.

- In this work, we have also investigated the fundamental frequencies of radial and vertical oscillations of test particles around the equatorial plane along stable circular orbits around a black hole in the presence of the aether field. It has been shown that the frequencies of Keplerian orbits and radial oscillations decrease with the increase in the absolute value of the aether parameter.
- As an application of fundamental frequencies, we considered the upper and lower frequencies of twin-peaked QPOs around the black holes. It has been shown that an increase in the absolute value of the aether parameter causes a decrease in the possible values of the frequency ratio. In this case, the QPO at the low-frequency regime will not be observed. We have also noted that the aether parameter cannot mimic the spin of the Kerr black hole, providing the same value of upper and lower frequencies in twin-peaked QPOs.
- Finally, using the observation data on observed twin peak QPOs and our numerical results, we obtained the constraints on the aether parameter (see Section 9 for the details).

Author Contributions: Conceptualization, J.R. and S.T.; methodology, J.R. and S.T.; software, S.T. and F.A.; validation, F.A. and F.H.; formal analysis, J.R. and A.A.; investigation, A.A., J.R. and F.H. All authors have read and agreed to the published version of the manuscript.

Funding: The research is supported in part by Grant No. F-FA-2021-510 of Agency of Innovative Development of the Uzbekistan and Erasmus + CZ OPAVA01. AA, JR. and FA acknowledge the Silesian University in Opava for hospitality.

Data Availability Statement: Not applicable.

Conflicts of Interest: The authors declare no conflict of interest.

References

1. Hořava, P. Quantum gravity at a Lifshitz point. *Phys. Rev. D* **2009**, *79*, 084008. [[CrossRef](#)]
2. Randall, L.; Sundrum, R. Large Mass Hierarchy from a Small Extra Dimension. *Phys. Rev. Lett.* **1999**, *83*, 3370–3373.
3. Afshordi, N. Gravitational Aether and the thermodynamic solution to the cosmological constant problem. *arXiv* **2008**, arXiv:0807.2639.
4. Prescod-Weinstein, C.; Afshordi, N.; Balogh, M.L. Stellar black holes and the origin of cosmic acceleration. *Phys. Rev. D* **2009**, *80*, 043513. [[CrossRef](#)]
5. Bambi, C. *Black Holes: A Laboratory for Testing Strong Gravity*; Springer: Singapore, 2017.
6. Chandrasekhar, S. *The Mathematical Theory of Black Holes*; Oxford University Press: New York, NY, USA, 1998.
7. Bambi, C. Testing the Kerr nature of stellar-mass black hole candidates by combining the continuum-fitting method and the power estimate of transient ballistic jets. *Phys. Rev. D* **2012**, *85*, 043002. [[CrossRef](#)]
8. Bambi, C.; Jiang, J.; Steiner, J.F. Testing the no-hair theorem with the continuum-fitting and the iron line methods: A short review. *Class. Quantum Gravity* **2016**, *33*, 064001. [[CrossRef](#)]
9. Zhou, M.; Cao, Z.; Abdikamalov, A.; Ayzenberg, D.; Bambi, C.; Modesto, L.; Nampalliwar, S. Testing conformal gravity with the supermassive black hole in 1H0707-495. *Phys. Rev. D* **2018**, *98*, 024007. [[CrossRef](#)]
10. Tripathi, A.; Yan, J.; Yang, Y.; Yan, Y.; Garnham, M.; Yao, Y.; Li, S.; Ding, Z.; Abdikamalov, A.B.; Ayzenberg, D.; et al. Constraints on the spacetime metric around seven “bare” AGN using X-ray reflection spectroscopy. *arXiv* **2019**, arXiv:1901.03064.
11. Wald, R.M. Black hole in a uniform magnetic field. *Phys. Rev. D* **1974**, *10*, 1680–1685. [[CrossRef](#)]
12. Aliev, A.N.; Galtsov, D.V.; Petukhov, V.I. Negative absorption near a magnetized black hole: Black hole masers. *Astrophys. Space Sci.* **1986**, *124*, 137–157. [[CrossRef](#)]
13. Aliev, A.N.; Gal'tsov, D.V. Reviews of Topical Problems: “Magnetized” black holes. *Sov. Phys. Uspekhi* **1989**, *32*, 75–92. [[CrossRef](#)]
14. Aliev, A.N.; Özdemir, N. Motion of charged particles around a rotating black hole in a magnetic field. *Mon. Not. R. Astron. Soc.* **2002**, *336*, 241–248. [[CrossRef](#)]
15. Stuchlík, Z.; Schee, J.; Abdujabbarov, A. Ultra-high-energy collisions of particles in the field of near-extreme Kehagias-Sfetsos naked singularities and their appearance to distant observers. *Phys. Rev. D* **2014**, *89*, 104048. [[CrossRef](#)]
16. Stuchlík, Z.; Kološ, M. Acceleration of the charged particles due to chaotic scattering in the combined black hole gravitational field and asymptotically uniform magnetic field. *Eur. Phys. J. C* **2016**, *76*, 32. [[CrossRef](#)]
17. Kovář, J.; Kopáček, O.; Karas, V.; Stuchlík, Z. Off-equatorial orbits in strong gravitational fields near compact objects II: Halo motion around magnetic compact stars and magnetized black holes. *Class. Quantum Gravity* **2010**, *27*, 135006. [[CrossRef](#)]
18. Kovář, J.; Slaný, P.; Cremaschini, C.; Stuchlík, Z.; Karas, V.; Trova, A. Electrically charged matter in rigid rotation around magnetized black hole. *Phys. Rev. D* **2014**, *90*, 044029. [[CrossRef](#)]

19. Stuchlík, Z.; Kološ, M.; Kovář, J.; Slaný, P.; Tursunov, A. Influence of Cosmic Repulsion and Magnetic Fields on Accretion Disks Rotating around Kerr Black Holes. *Universe* **2020**, *6*, 26. [[CrossRef](#)]
20. de Felice, F.; Sorge, F. Magnetized orbits around a Schwarzschild black hole. *Class. Quantum Gravity* **2003**, *20*, 469–481.
21. de Felice, F.; Sorge, F.; Zilio, S. Magnetized orbits around a Kerr black hole. *Class. Quantum Gravity* **2004**, *21*, 961–973. [[CrossRef](#)]
22. Rahimov, O.G.; Abdujabbarov, A.A.; Ahmedov, B.J. Magnetized particle capture cross section for braneworld black hole. *Astrophys. Space Sci.* **2011**, *335*, 499–504. [[CrossRef](#)]
23. Narzilloev, B.; Rayimbaev, J.; Shaymatov, S.; Abdujabbarov, A.; Ahmedov, B.; Bambi, C. Can the dynamics of test particles around charged stringy black holes mimic the spin of Kerr black holes? *Phys. Rev. D* **2020**, *102*, 044013. [[CrossRef](#)]
24. Vrba, J.; Abdujabbarov, A.; Kološ, M.; Ahmedov, B.; Stuchlík, Z.; Rayimbaev, J. Charged and magnetized particles motion in the field of generic singular black holes governed by general relativity coupled to nonlinear electrodynamics. *Phys. Rev. D* **2020**, *101*, 124039. [[CrossRef](#)]
25. Vrba, J.; Abdujabbarov, A.; Tursunov, A.; Ahmedov, B.; Stuchlík, Z. Particle motion around generic black holes coupled to non-linear electrodynamics. *Eur. Phys. J. C* **2019**, *79*, 778. [[CrossRef](#)]
26. Ingram, A.; van der Klis, M.; Middleton, M.; Done, C.; Altamirano, D.; Heil, L.; Uttley, P.; Axelsson, M. A quasi-periodic modulation of the iron line centroid energy in the black hole binary H1743-322. *Mon. Not. R. Astron. Soc.* **2016**, *461*, 1967–1980. [[CrossRef](#)]
27. Stuchlík, Z.; Kotrlová, A.; Török, G. Multi-resonance orbital model of high-frequency quasi-periodic oscillations: Possible high-precision determination of black hole and neutron star spin. *Astron. Astrophys.* **2013**, *552*, A10. [[CrossRef](#)]
28. Toshmatov, B.; Stuchlík, Z.; Ahmedov, B. Generic rotating regular black holes in general relativity coupled to nonlinear electrodynamics. *Phys. Rev. D* **2017**, *95*, 084037. [[CrossRef](#)]
29. Stella, L.; Vietri, M. Lense-Thirring Precession and Quasi-periodic Oscillations in Low-Mass X-Ray Binaries. *Astrophys. J. Lett.* **1998**, *492*, L59–L62. [[CrossRef](#)]
30. Rezzolla, L.; Yoshida, S.; Maccarone, T.J.; Zanotti, O. A new simple model for high-frequency quasi-periodic oscillations in black hole candidates. *Mon. Not. R. Astron. Soc.* **2003**, *344*, L37–L41. [[CrossRef](#)]
31. Stuchlík, Z.; Kotrlová, A.; Török, G. Resonant radii of kHz quasi-periodic oscillations in Keplerian discs orbiting neutron stars. *Astron. Astrophys.* **2011**, *525*, A82. [[CrossRef](#)]
32. Török, G.; Kotrlová, A.; Srámková, E.; Stuchlík, Z. Confronting the models of 3:2 quasiperiodic oscillations with the rapid spin of the microquasar GRS 1915+105. *Astron. Astrophys.* **2011**, *531*, A59. [[CrossRef](#)]
33. Silbergleit, A.S.; Wagoner, R.V.; Ortega-Rodríguez, M. Relativistic Diskoseismology. II. Analytical Results for C-modes. *Astrophys. J.* **2001**, *548*, 335–347. [[CrossRef](#)]
34. Wagoner, R.V.; Silbergleit, A.S.; Ortega-Rodríguez, M. “Stable” Quasi-periodic Oscillations and Black Hole Properties from Diskoseismology. *Astrophys. J. Lett.* **2001**, *559*, L25–L28. [[CrossRef](#)]
35. Rayimbaev, J.; Majeed, B.; Jamil, M.; Jusufi, K.; Wang, A. Quasiperiodic oscillations, quasinormal modes and shadows of Bardeen-Kiselev Black Holes. *Phys. Dark Universe* **2022**, *35*, 100930. [[CrossRef](#)]
36. Stuchlík, Z.; Vrba, J. Epicyclic Oscillations around Simpson-Visser Regular Black Holes and Wormholes. *Universe* **2021**, *7*, 279. [[CrossRef](#)]
37. Stuchlík, Z.; Vrba, J. Epicyclic orbits in the field of Einstein–Dirac–Maxwell traversable wormholes applied to the quasiperiodic oscillations observed in microquasars and active galactic nuclei. *Eur. Phys. J. Plus* **2021**, *136*, 1127. [[CrossRef](#)]
38. Stuchlík, Z.; Vrba, J. Supermassive black holes surrounded by dark matter modeled as anisotropic fluid: Epicyclic oscillations and their fitting to observed QPOs. *J. Cosmol. Astropart. Phys.* **2021**, *2021*, 059. [[CrossRef](#)]
39. Bian, W.H.; Zhao, Y.H. Accretion Rates and the Accretion Efficiency in AGNs. *Publ. Astron. Soc. Jpn.* **2003**, *55*, 599–603. [[CrossRef](#)]
40. Stella, L. The relativistic precession model for QPOs in low mass X-ray binaries. In *Proceedings of the X-ray Astronomy: Stellar Endpoints, AGN, and the Diffuse X-ray Background, Bologna, Italy, 6–10 September 2001*; American Institute of Physics Conference Series; White, N.E., Malaguti, G., Palumbo, G.G.C., Eds.; Curran Associates, Inc.: Nice, France, 2001; Volume 599, pp. 365–376. [[CrossRef](#)]
41. Ingram, A.; Motta, S. Solutions to the relativistic precession model. *Mon. Not. R. Astron. Soc.* **2014**, *444*, 2065–2070. [[CrossRef](#)]
42. Abramowicz, M.A.; Kluźniak, W. A precise determination of black hole spin in GRO J1655-40. *Astron. Astrophys.* **2001**, *374*, L19–L20. [[CrossRef](#)]
43. Kato, S. Resonant Excitation of Disk Oscillations by Warps: A Model of kHz QPOs. *Publ. Astron. Soc. Jpn.* **2004**, *56*, 905–922. [[CrossRef](#)]
44. Kato, S. Frequency Correlation of QPOs Based on a Resonantly Excited Disk-Oscillation Model. *Publ. Astron. Soc. Jpn.* **2008**, *60*, 889. [[CrossRef](#)]
45. Stella, L.; Vietri, M.; Morsink, S.M. Correlations in the Quasi-periodic Oscillation Frequencies of Low-Mass X-ray Binaries and the Relativistic Precession Model. *Astrophys. J.* **1999**, *524*, L63–L66. [[CrossRef](#)]
46. Bambi, C. Testing the nature of the black hole candidate in GRO J1655-40 with the relativistic precession model. *arXiv* **2013**, arXiv:1312.2228.
47. Belloni, T.; Soleri, P.; Casella, P.; Méndez, M.; Migliari, S. High-frequency quasi-periodic oscillations from GRS 1915+105 in its C state. *Mon. Not. R. Astron. Soc.* **2006**, *369*, 305–310. [[CrossRef](#)]

Disclaimer/Publisher’s Note: The statements, opinions and data contained in all publications are solely those of the individual author(s) and contributor(s) and not of MDPI and/or the editor(s). MDPI and/or the editor(s) disclaim responsibility for any injury to people or property resulting from any ideas, methods, instructions or products referred to in the content.